



Enhancing dielectric properties of ZnO nanopowders with 2D hBN doping: production, structural, morphological and dielectric characterization

Cihan Ozel¹ · Cevher Kursat Macit⁶ · Turan Gurgenc² · Fatih Biryancı³ · Ezgi Gurgenc⁴ · Stefano Bellucci⁵

Received: 19 July 2023 / Accepted: 11 February 2024 / Published online: 15 March 2024
© The Author(s) 2024

Abstract

In this study, it was aimed to improve the dielectric properties of ZnO nanoparticles with the addition of hBN, which was not previously available in the literature, and thus to expand their usage areas. Sol–gel synthesis method was used in this study to create pure and hexagonal boron nitride (hBN) doped zinc oxide (ZnO) nanoparticles. Zinc acetate dihydrate $Zn(CH_3COO)_2 \cdot 2H_2O$, sodium hydroxide NaOH, and hexagonal boron nitride (hBN), all from Sigma Aldrich, were used as starting reagents. The reagents were dissolved during the sol–gel synthesis by being heated to 90 °C for 4 h in a magnetic stirrer. FT-IR, XRD, FE-SEM, EDX characterization techniques, and impedance analyzer were used to find functional groups, structural, morphological, and chemical composition, and dielectric properties of the nanoparticles, respectively. The produced un-doped and hBN-doped ZnO particles consist of nano-sized structures. Changes occurred in the intensities and locations of the XRD diffraction peaks and FT-IR peaks with the addition of hBN. Characteristic peaks of both ZnO and hBN were observed in the diffraction peaks of the doped nanoparticles. All nanoparticles were of high purity and were successfully produced by the sol–gel method. It was shown that as the hBN doping level increased, there were more hBN nanoplates in the ZnO matrix, and the EDX results also showed an increase in hBN addition. The frequency stability of the dielectric properties improved after hBN doping. While the dielectric constant at 1 kHz frequency at room temperature is 12.07 in pure ZnO nanoparticles, the increase up to 55.21 is observed in 10% hBN doped nanocomposites. This situation is considered as a great potential for technological applications of this novel nanocomposite material.

Keywords Semiconductor · Nanomaterial · Ceramics · Zinc oxide · Hexagonal boron nitride · Dielectric

1 Introduction

Nano-sized materials are attracting a lot of attention today due to their potential to add new properties to existing materials and to apply them to different technologies [1–5]. During the production of nanomaterials, significant studies are carried out to control the structural and morphological properties [5–9].

Metal oxide semiconductors (MOS) are crucial in a variety of scientific disciplines, including chemistry, physics, medicine, and engineering, due to their unique electrical, optical, and magnetic characteristic [10, 11]. Due to its distinctive and new uses in optics, optoelectronics, catalysis, and piezoelectricity, research into functional oxide-based, one-dimensional nanostructures has rapidly grown since the discovery of oxide nanobelts of semiconductor oxides. An extensive range of materials with varied chemical compositions and crystallographic structures have been thoroughly

✉ Cihan Ozel
cozel@firat.edu.tr

¹ Department of Mechanical Engineering, Firat University, Faculty of Engineering, 23119 Elazig, Turkey

² Department of Automotive Engineering, Firat University, Faculty of Technology, 23119 Elazig, Turkey

³ Department of Chemistry, Firat University, Faculty of Science, 23119 Elazig, Turkey

⁴ Department of Mechanical Engineering, Firat University, Faculty of Technology, 23119 Elazig, Turkey

⁵ INFN-Laboratori Nazionali di Frascati, Via E. Fermi 54, 00044 Frascati, Italy

⁶ School of Aviation, Aircraft Airframe-Engine Maintenance, Firat University, 23119, Elazig, Turkey

studied for using a special class of semi-one-dimensional nanomaterials known as semiconductor oxide nanoparticles [10].

Zinc oxide (ZnO), a unique natural n-type semiconductor among semiconductor materials, has exceptional chemical stability, broad and direct band gap (3.37 eV), high exciton binding energy (60 meV) at room temperature and high exciton binding energy at low temperatures characteristic [10, 11]. ZnO has a hexagonal structure with cell parameters $a=b=3.250$ and $c=5.206$ Å, [4, 5]. Due to its properties, ZnO is used in a wide range of applications, including as ultraviolet (UV) light emitters, piezoelectric devices, chemical and gas sensors, transistors, solar cells, catalysts, and spintronics [7–9, 12–15]. To date, various methods have been used to create nanostructured ZnO powders with different morphologies and ionic additions for fundamental research. Numerous ions were identified to improve the optical, electrical, and catalytic properties of ZnO powder, increasing the material potential for use in technology [14–20].

Because of its essential application, nanotechnology has played a significant role in all areas of science for the past 20 years. The two-dimensional material (2D-mats) created in this period, graphene, has exceptional chemical and thermal properties, but more critically, exceptional solution workability to enhance dye degradation [21–24]. Hexagonal boron nitride (hBN), often known as “white graphene,” has a huge surface area and a polar B and N bond (B-N), which gives it outstanding adsorption characteristics against a variety of dyes, metallic ions, and organic contaminants [25, 26]. A 2-dimensional nanostructure with significant mechanical, electrical, and chemical characteristics is called hBN [27]. It is a substance based on hexagonal covalent bonds between nitrogen and boron atoms [28]. Between the layers, there are flimsy Van der Waals bonds [29]. It possesses exceptional qualities such as chemical inertness, high thermal conductivity, excellent thermal shock resistance, low thermal expansion, high electrical resistance, low dielectric constant, and non-toxicity [30–32]. Various techniques, such as sol–gel, microemulsion, chemical and hydrothermal and precipitation methods, thermal decomposition of organic precursors, spray pyrolysis, electro-deposition, ultrasonic and microwave-assisted techniques, were used to obtain high-quality nanomaterials [11, 33–35].

Particularly important in the creation of nanocomposites is the sol–gel process. Due to the fact that, as compared to materials made using conventional techniques, sol–gel preparation offers a larger specific surface area, superior homogeneity and purity, better microstructure control for metallic particles, a narrower pore size, and uniform particle dispersion. The simplicity, cheap cost, reproducibility, and capacity to produce uniform, well-adhered films are the key benefits of the sol–gel process [36–39].

The literature has reported on the dielectric constant, dielectric loss factors, and conductivity properties of different compounds and these properties are one of the most important properties used in the usage areas of solid materials [40–45]. Knowing the dielectric constant and dissipation factor properties, which provide very important information about the physical and chemical properties of materials, has a very important place in electronic device design. In addition, the distribution of polar groups as well as the dielectric properties of the compounds that make up the materials can be controlled with their statistical basic behavior [46]. Numerous multifunctional electronic and optoelectronic devices could use these dielectric characteristics of materials [47–50].

Numerous studies have recently concentrated on the idea that dopant presence can alter ZnO’s dielectric behavior [51–53]. According to the research findings, the dielectric constant values of metal-doped ZnO are lower than those of undoped ZnO bulk materials, and they decrease as the doping level increases [54–57].

It is well known that hBN has a strong thermal conductivity and a comparatively low dielectric constant. The crystalline structure of hBN is reflected in its plate-like shape, and both the dielectric and thermal characteristics are highly anisotropic [58–60]. When it comes to electrical resistance and dielectric loss, it was found that hBN nanocomposite materials outperform metallic fillers and carbon nanoparticles [58, 61].

The main purpose of this study is to expand the usage areas of ZnO semiconductor metal oxide, which is used in many electronic, optoelectronic and electrochemical technologies, by improving its dielectric properties. In current study, un-doped and doped ZnO nanocomposites with (1, 5, 10 wt%) hBN were fabricated by sol–gel method, and in our knowledge such composites were not produced before. When the literature studies of ZnO semiconductor nanoparticles are examined, it is seen that the improvement of dielectric and electrical properties can be improved by synthesizing with new reinforcing elements or materials. FT-IR, XRD, FE-SEM and EDX characterization techniques were used to find functional groups, structural, morphological and chemical composition properties of the nanoparticles, respectively. Also, the dielectric properties of the produced nanoparticles were analyzed and interpreted.

2 Materials and methods

2.1 Synthesis of nanoparticles

Sol–gel synthesis method was used in this study to create pure and hexagonal boron nitride (hBN) doped zinc oxide (ZnO) nanoparticles. Zinc acetate dihydrate

Fig. 1 Production steps of nanoparticle fabrication

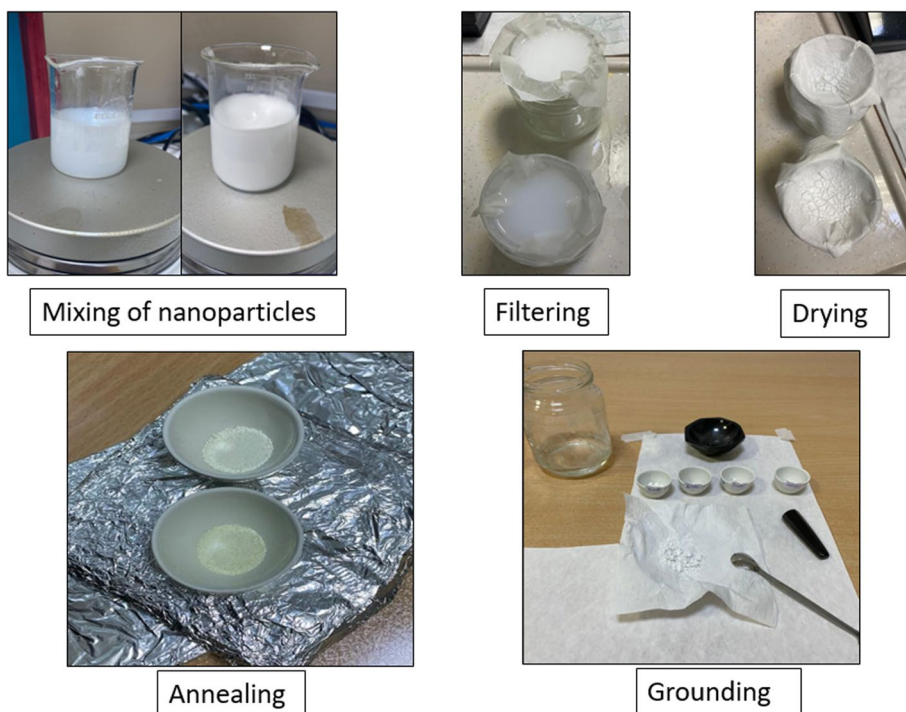
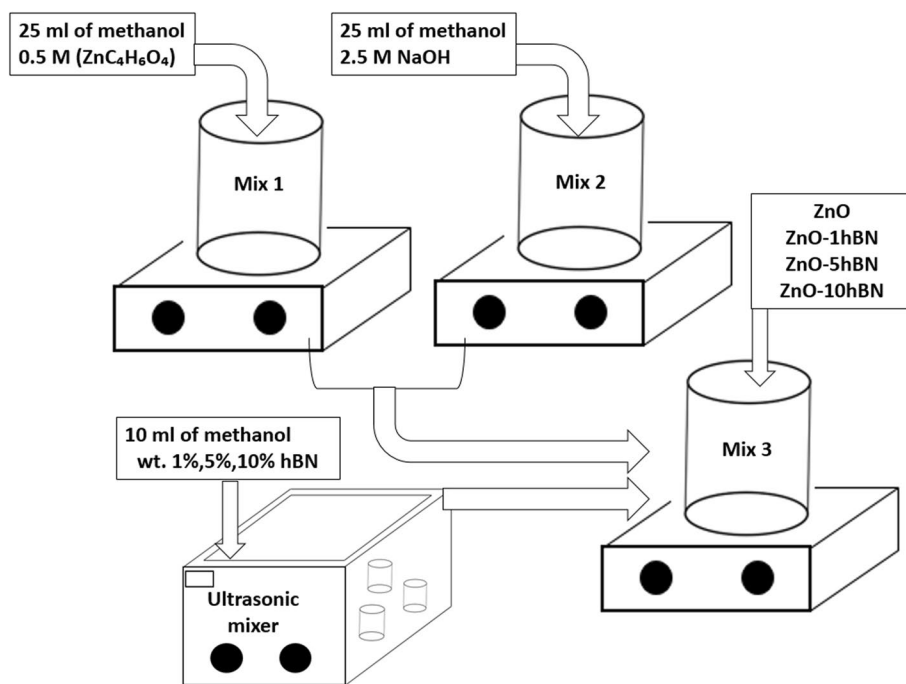


Fig. 2 Scheme of nanoparticle production



Zn(CH₃COO)₂·2H₂O), sodium hydroxide NaOH, and hexagonal boron nitride (hBN), all from Sigma Aldrich, were used as starting reagents. The production steps and production scheme of ZnO and hBN-reinforced ZnO nanoparticles are shown in Figs. 1 and 2, respectively. The notation and additive amounts of the produced nanoparticles are given in Table 1. Literature studies were also used during the synthesis of nanoparticles [62]. Detailed information about

Table 1 Sample notation and composition

Sample	Content
ZnO	Pure ZnO
ZnO-1hBN	1% hBN doped ZnO
ZnO-5hBN	5% hBN doped ZnO
ZnO-10hBN	10% hBN doped ZnO

the production of pure ZnO nanoparticles was previously given in detail in the study carried out by researchers in our research team [35]. As a difference, nano-sized hBN particles were used as additive materials in this study and all other processes were carried out in the same way as in the related study. 1, 5, and 10 wt% were chosen as the contribution rate. Since hBN is chemically inert and insulating, the contribution rate was limited to 10% in order not to limit the working area too much [63, 64]. To ensure homogeneity, three samples were produced from each sample and analyzes were performed after the produced nanoparticles were mixed with each other.

2.2 Characterization of nanoparticles

Detailed information about the structural, morphological and electrical characterizations of un-doped and doped ZnO nanoparticles was previously given in detail in the study carried out by researchers in our research team [35]. Detailed information about the devices used is given in the relevant study and will be briefly mentioned here. The functional groups of un-doped and hBN-doped ZnO nanoparticles were investigated by FT-IR analysis at wavenumber range of 4000–500 cm^{-1} . Structural properties of fabricated all nanoparticles were investigated by XRD technique. XRD diffraction patterns were recorded under $\text{CuK}\alpha$ ($\lambda = 1.5406 \text{ \AA}$) radiation over $2\theta = 20$ to 80° scanning range and 40 kV/40 mA. Important structural properties of the produced nanoparticles, such as the lattice parameters ($a = b$ and c), volumes of unit cells (V), crystalline size (D) and average

crystalline size, were calculated using XRD diffraction patterns and equations detailed in literature researches [22–24, 65–71]. Morphological properties and chemical composition of all nanoparticles were investigated by FE-SEM and EDX techniques, respectively. Impedance analyzer was used to analyze dielectric readings in the frequency range of 1000–20000 Hz. By using the capacitance, dielectric loss factor and conductance values recorded at room temperature, the dielectric properties were calculated with the help of equation given in literature researches [42, 46, 72].

3 Results and discussion

3.1 Characterization of synthesized ZnO-hBN nanoparticles

In the FT-IR spectra seen in Fig. 3, the peaks at 383, 407, 480, 512 and 582 cm^{-1} are correspondent to Zn–O bonding [73, 74]. The vibration at 886 cm^{-1} is thought to be a substituted hydrogen bond at the oxygen site (HO) attached to the lattice site of Zn (i.e., Zn–HO). For ZnO nanoparticles, these peaks correspond to the polar stretch vibration modes A1 (TO), E1 (TO), A1 (LO), and E1 (LO), respectively. Two core B–N peaks were found in FT-IR spectra at 786 and 1342 cm^{-1} , and they were attributed to B–N–B bending vibrations and B–N stretched vibration. The last peak was associated with the bending vibration A_{2u} mode (out-of-plane), while the previous peak was found to be well-matched with the stretching vibration E_{1u} mode (in-plane)

Fig. 3 FT-IR spectra of the synthesized samples

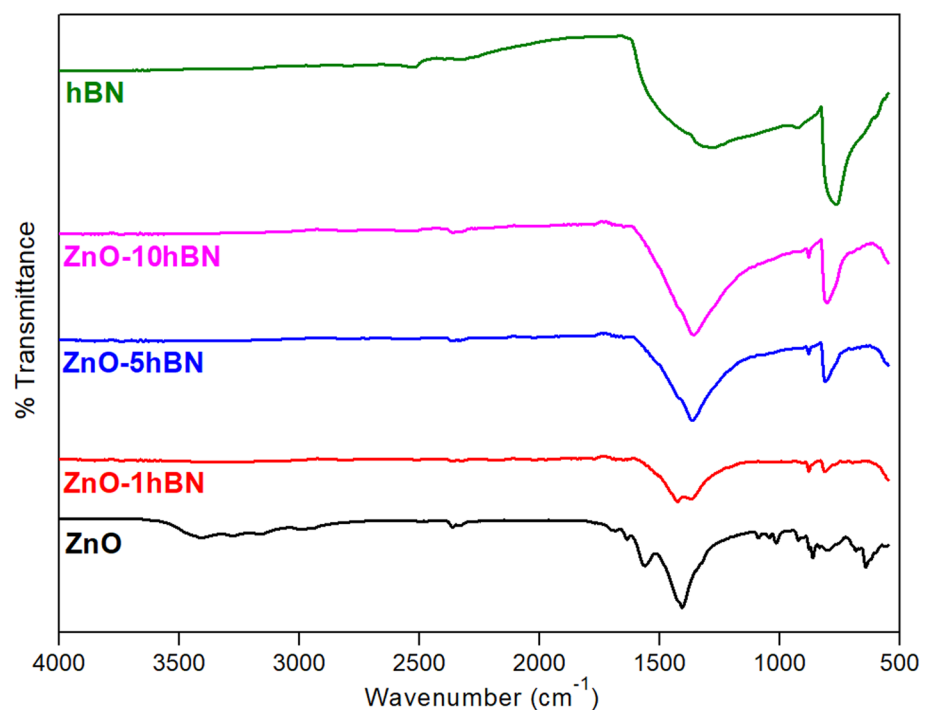


Fig. 4 XRD diffraction patterns of synthesized nanoparticles

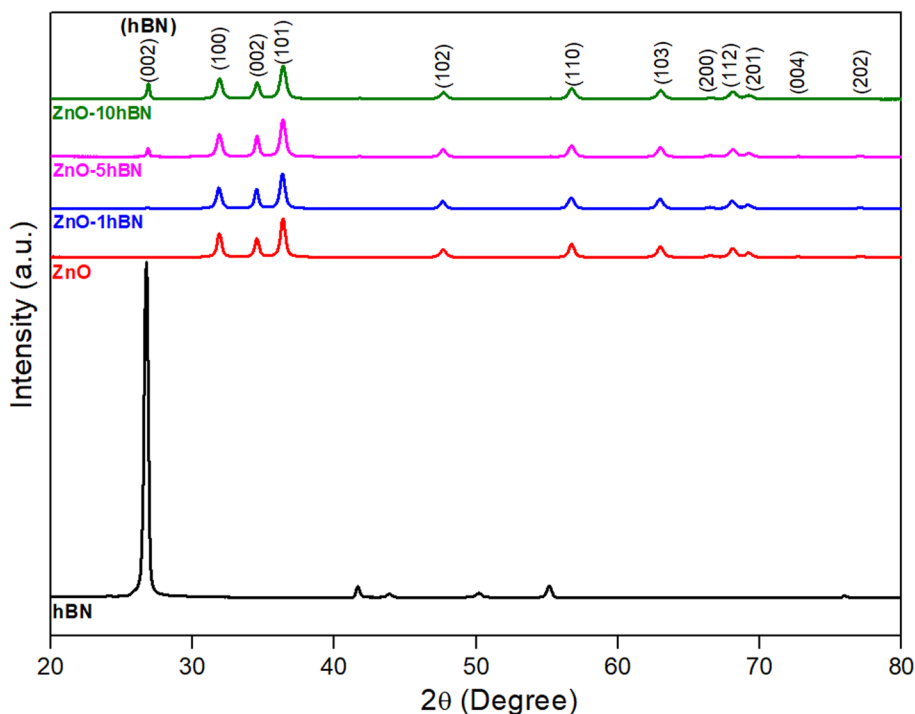


Table 2 The 2θ values of the diffraction planes of the synthesized nanoparticles

Sample/ Diffraction plane	hBN	ZnO	ZnO-1hBN	ZnO-5hBN	ZnO-10hBN
(002) hBN	26.754	–	26.804	26.865	26.890
(100)	–	31.898	31.851	31.888	31.913
(002)	–	34.524	34.511	34.548	34.560
(101)	–	36.382	36.380	36.382	36.389
(102)	–	47.681	47.637	47.661	47.661
(110)	–	56.740	56.692	56.705	56.742
(103)	–	62.964	62.952	62.977	62.989
(200)	–	66.509	66.404	66.515	66.515
(112)	–	68.085	68.024	68.086	68.098
(201)	–	69.188	69.224	69.249	69.323
(004)	–	72.654	72.688	72.713	72.861
(202)	–	77.226	77.068	77.092	77.030

Table 3 The calculated a, c and V values of synthesized nanoparticles

Sample	2 theta (101)	a=b (Å)	c (Å)	V (Å ³)
ZnO	36.382	3.225	5.266	47.435
ZnO-1hBN	36.380	3.225	5.267	47.443
ZnO-5hBN	36.382	3.225	5.267	47.435
ZnO-10hBN	36.389	3.224	5.265	47.409

Table 4 Average crystalline sizes of produced nanoparticles

Average crystalline size (nm)	ZnO	ZnO-1hBN	ZnO-5hBN	ZnO-10hBN
D (100)	19.846	18.310	18.156	16.988
D (002)	19.845	22.628	22.367	17.661
D (101)	18.953	17.959	17.571	15.982
D (102)	17.045	17.113	16.845	15.256
D (110)	17.371	15.092	14.782	14.302
D (103)	15.572	14.700	14.223	12.938
D (200)	17.175	8.8708	8.631	8.019
D (112)	15.222	13.421	13.044	12.720
D (201)	14.545	12.105	11.823	11.455
D (004)	5.821	1.826	1.828	1.854
D (202)	0.533	0.681	0.642	0.649
D _{ave}	14.720	12.973	12.719	11.620

[75–78]. It was shown that, as the amount of hBN addition increased, the hBN peak intensities also increase.

XRD patterns of the synthesized un-doped and hBN-doped ZnO nanoparticles are shown in Fig. 4 and 2θ values are given in Table 2. Tables 3 and 4 show, a=b, c, V, and D values, and average crystalline size of produced nanoparticles, respectively. Detailed analysis results regarding the XRD analysis of un-doped ZnO nanoparticles were given in detail in our previous study [35], and in present study they are briefly mentioned again to show the effect of the hBN additive. In pure ZnO nanoparticles, high intensity

peaks were observed at 31.898° , 34.524° , 36.382° , 47.681° , 56.740° , 62.964° , 66.509° , 68.085° , 69.188° , 72.654° and 77.226° 2θ degrees, and these peaks are the characteristic peaks of ZnO [35, 73, 79]. These peaks are correspondent to (100), (002), (101), (102), (110), (103), (200), (112), (201), (004) and (202) planes, respectively [74–77]. In the hBN-doped samples, besides the characteristic peaks belonging to pure ZnO, the characteristic peak of hBN at 26.754° 2θ is observed and this peak corresponds to the (002) plane [80, 81]. It is seen that the (002) peak intensity increases as the hBN content increases. It is the same as the reflection of the hexagonal graphite structure (002) observed at $2\theta \sim 26^\circ$ [82]. It was observed that the 2θ values shifted with the increase of hBN content. The standard values (JCPDS Card No. 36-1451) regarding the scanning rate are in agreement with the lattice constants a and c of un-doped and Hbn-doped ZnO nanoparticles given in Table 3. The analysis

results show that the characteristic features of hBN and ZnO are remained. The XRD results obtained for the nanoparticles, whose production and analysis were completed, show that the hBN component is combined with ZnO.

The a (\AA), c (\AA), and V (\AA^3) values calculated using XRD patterns are shown in Table 4. The calculated all this values are very close to the literature studies of ZnO [83–86]. With the increase in the amount of hBN addition to ZnO nanoparticles, the cell parameters and unit cell volume decrease. It was also seen in the literature studies that reductions in cell parameters occur in doped ZnO nanoparticles [87, 88]. Similarly, it is seen that the mean crystal size of the synthesized nanoparticles decreases with the increase in the amount of hBN reinforcement nanoparticles [87, 88].

The FE-SEM images and EDX analysis results are shown in Figs. 5, 6, 7, 8, 9. In FE-SEM analysis, it was observed that ZnO nanoparticles formed on the hBN

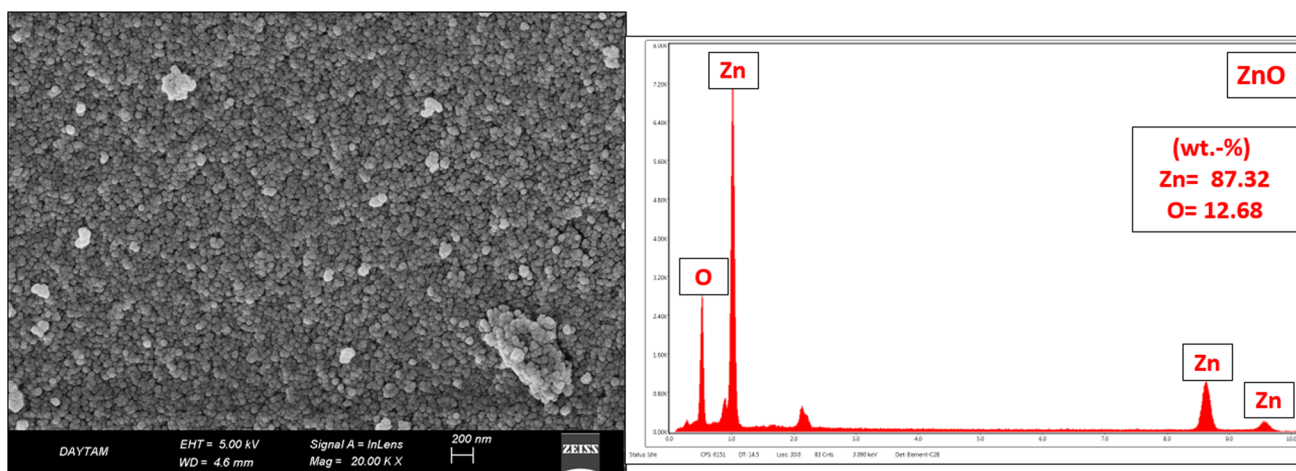


Fig. 5 FE-SEM images of ZnO nanoparticles

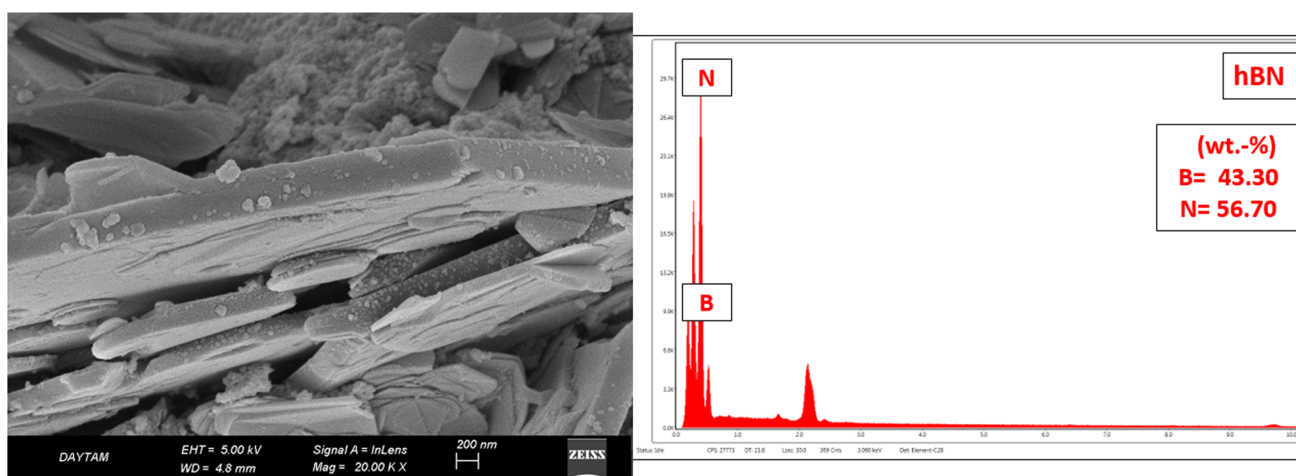


Fig. 6 FE-SEM images of hBN nanoparticles

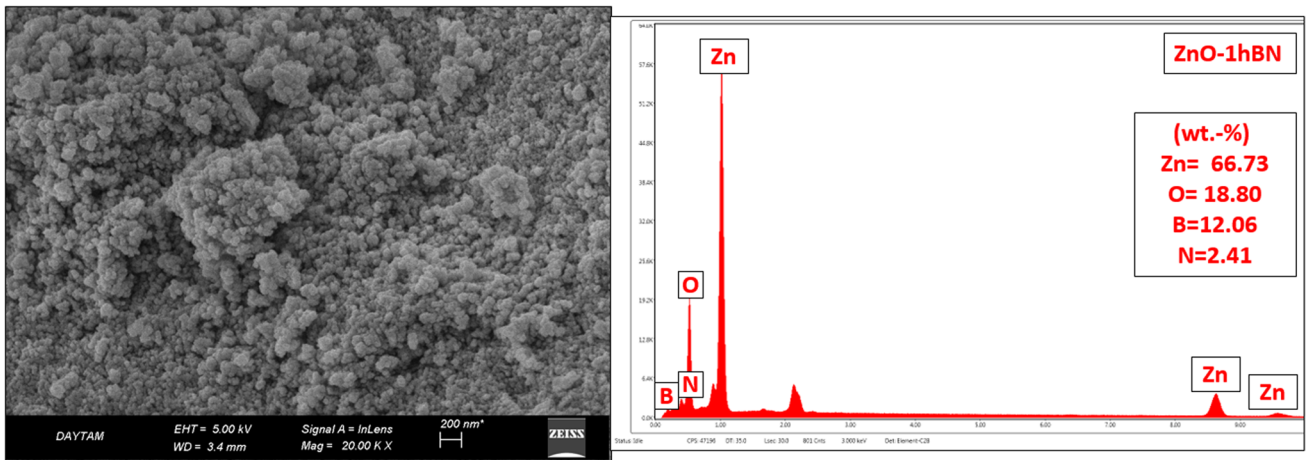


Fig. 7 FE-SEM images of ZnO-1hBN nanoparticles

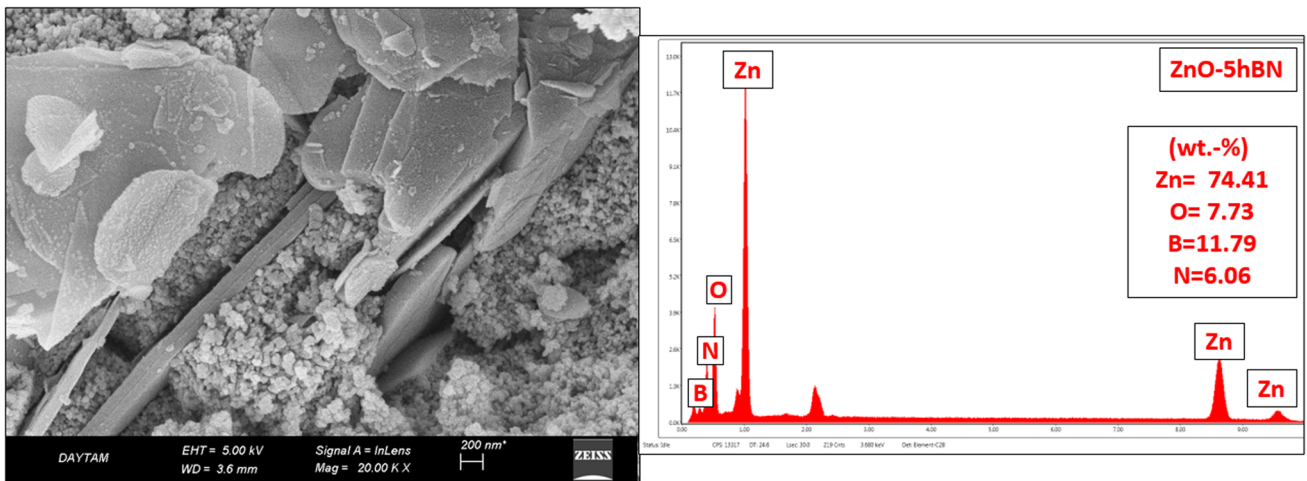


Fig. 8 FE-SEM images of ZnO-5hBN nanoparticles

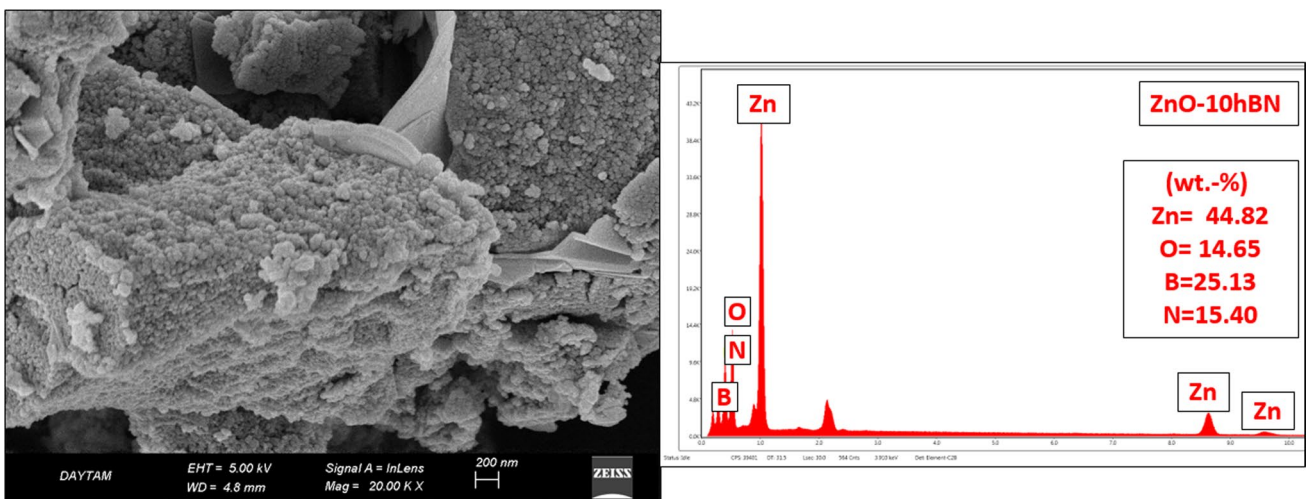


Fig. 9 FE-SEM images of ZnO-10hBN nanoparticles

nanoplates. With the increase in the amount of hBN adding, the size of the hBN plates increased and ZnO nanoparticles were formed on the surface of the hBN. The presence of platelet-like particles is observed in all hBN-doped samples. This situation also draws attention in the literature [89–91]. As a result of EDX analysis, increases in the amounts of B and N were observed with the increase in the

doping ratio. In the EDX analysis results, it was observed that Zn, O, N and B elements are present in the samples.

3.2 Dielectric properties

The dielectric constant, dielectric loss and conductivity values of the produced nanoparticles are shown in Figs. 10, 11, 12. While the dielectric constant values given in Fig. 8

Fig. 10 The variation of the dielectric constant vs. frequency of synthesized nanoparticles

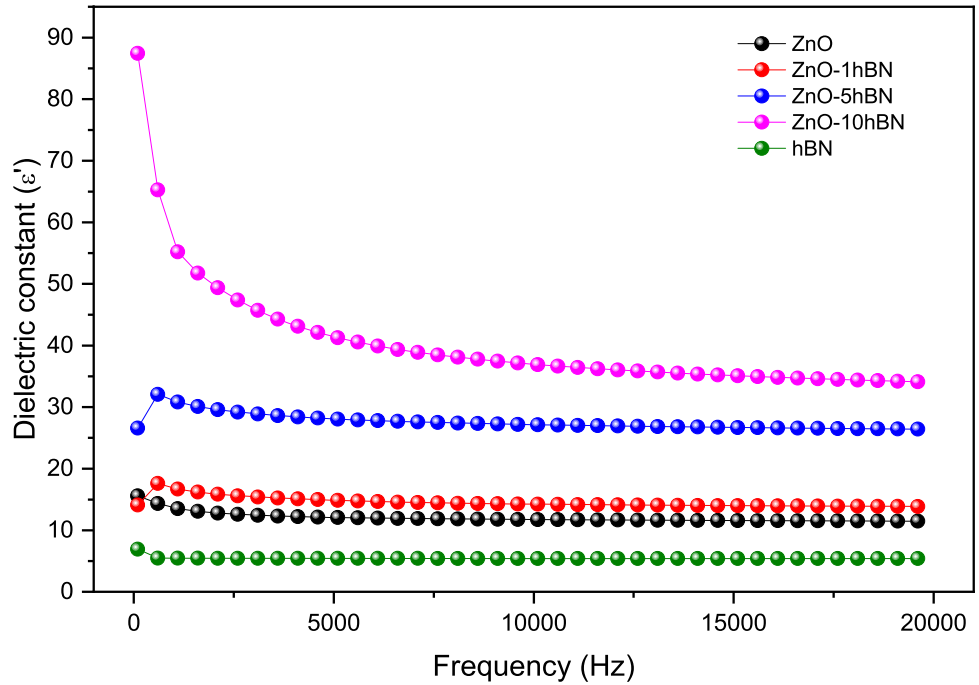


Fig. 11 The variation of the dielectric loss vs. frequency of synthesized nanoparticles

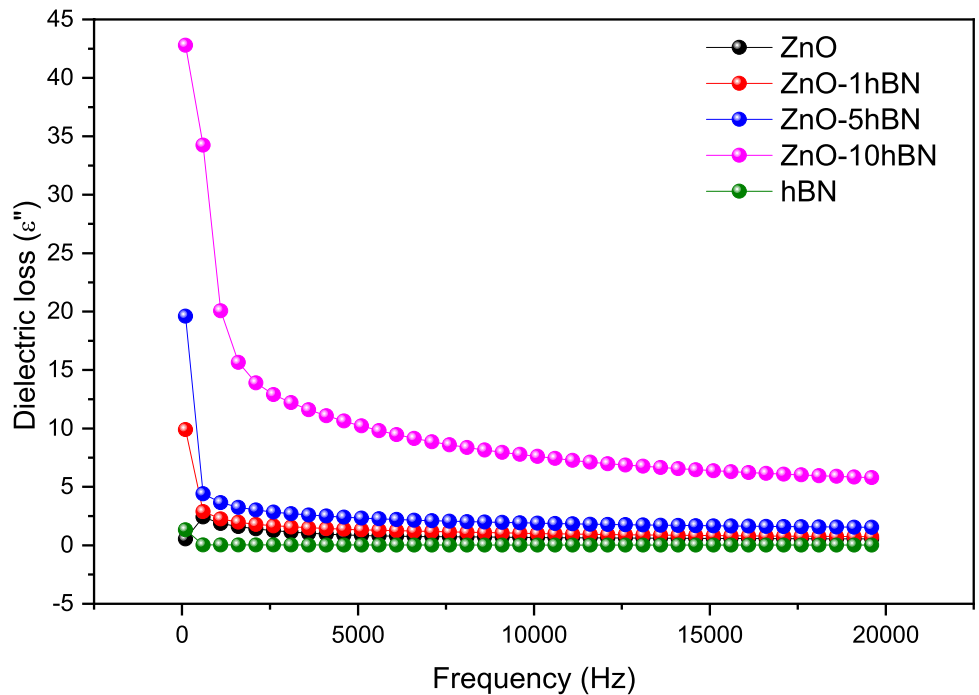
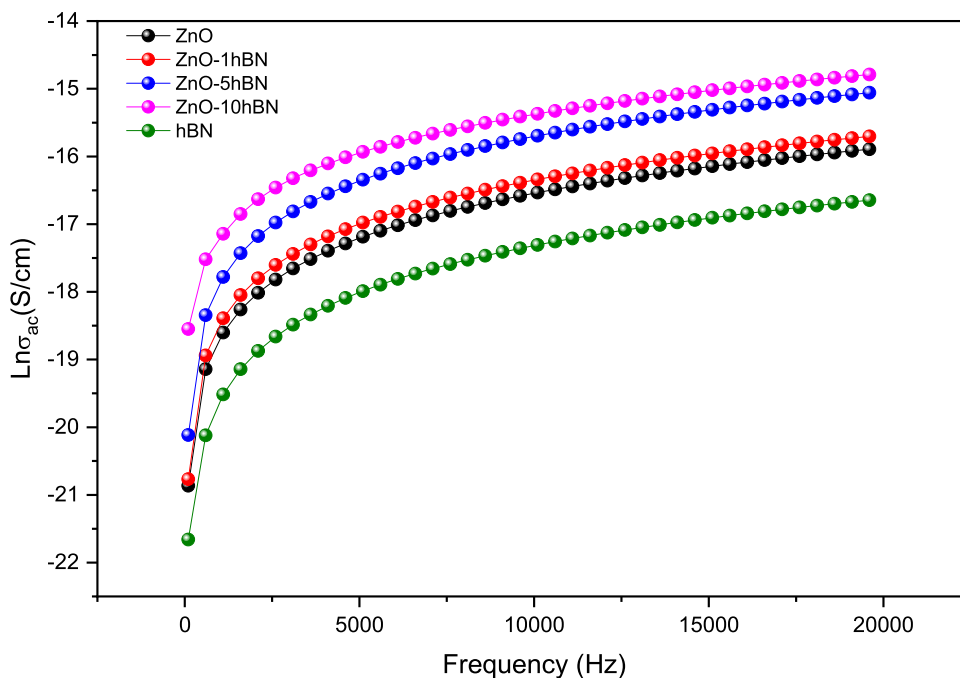


Fig. 12 The variation of the conductivity vs. frequency of synthesized nanoparticles



show sudden decreases at low frequencies, they approach almost constant values at higher frequencies. This is due to the fact that dipoles tend to be more directional in the low frequency region. The dielectric test was replicated five different times at room temperature for each samples. The standard deviation and coefficient of variation of the dielectric parameters at 1 kHz for each composite were calculated and summarized in Table 5. The coefficient of variation for the dielectric constant ranges from 1.26 to 3.07, while for the dielectric loss it ranges from 1.36 to 6.25. In addition, while the dielectric constant at 1 kHz frequency at room temperature is 12.07 ± 0.224 for pure ZnO, it has increased to 55.21 ± 0.726 in 10% hBN added composite. This is thought to be due to the increased interfacial polarization between ZnO and hBN [92–96]. The measurement accuracy varies accordingly with sample thickness and spectral position. The data quality of this five-sample average indicates not only the adequacy of the experimental approach, but also excellent sample homogeneity. As can be clearly seen in

the graph in Fig. 10, the conductivity values increased with increasing hBN content. Also the frequency stability of the dielectric properties improved after hBN doping. The conductivity value of ZnO in its pure form is 8.35×10^{-09} S/cm, and when 10% hBN is added, it is determined as 3.59×10^{-08} S/cm. When the literature studies are examined, it has been reported that the hBN additive affects the dielectric properties positively, as in this study [97–99]. In studies investigating the dielectric properties of undoped or doped ZnO nanoparticles with different elements, dielectric constants varied between 7 and 10.26, and dielectric loss values varied between 0.04 and 0.212 [100–103]. In our study, these values are between 12.070–55.219 and 0.840–20.075 for dielectric constant and dielectric loss, respectively. While the dielectric constant at 1 kHz frequency at room temperature is 12.07 in pure ZnO nanoparticles, the increase up to 55.21 is observed in 10% hBN doped nanocomposites. The high dielectric constant shows that the nanocomposite particles produced have potential for use in the semiconductor

Table 5 Dielectric parameters of samples at room temperature at 1 kHz

Sample	Dielectric constant (ϵ')	SD (COV)	Dielectric loss (ϵ'')	SD (COV)	AC conductivity μ S/cm	SD (COV)	Log σ_{ac} (S/cm)
ZnO	12.070	0.224 (1.85%)	0.840	0.004 (4.76%)	0.00835	0.00111 (13.31%)	- 8.070
hBN	5.462	0.168 (3.07%)	0.032	0.002 (6.25%)	0.00334	0.00029 (8.71%)	- 19.516
ZnO-1hBN	16.704	0.257 (1.53%)	2.253	0.084 (3.72%)	0.01030	0.00093 (9.12%)	- 18.390
ZnO-5hBN	30.808	0.391 (1.26%)	3.652	0.109 (2.98%)	0.01900	0.00115 (6.08%)	- 17.801
ZnO-10hBN	55.219	0.726 (1.31%)	20.075	0.281 (1.39%)	0.03590	0.00105 (2.95%)	- 17.141

* ϵ' is dielectric constant; ϵ'' is dielectric loss factor; SD is standard deviation; and COV is coefficient of variation

electronics industry. The dielectric parameters indicate that, regardless of the contribution of the crystalline phases, perceived porosity might be the main factor in determining the relative dielectric constant values. But the hBN to ceramic bands' platelet-like crystal structure also contributes significantly to the dielectric response. It shows that, despite high apparent porosity, which lowers the material relative dielectric constant, high apparent porosity does not prevent the material from being employed as a high-frequency substrate. The latency of electromagnetic signals transmitted by high frequency devices is therefore decreased by integrating with hBN study [97–99, 104]. As a result, multilayer hBN doped ceramic tapes are considered to be a crucial high-frequency substrate for electronic transmission devices.

4 Conclusions

When the structural and morphological analyses of the nanoparticles produced by the sol–gel synthesis method were completed, it was observed that the ZnO nanoparticles and the hBN reinforced ZnO nanoparticles were combined at nanoscale and successfully synthesized. The distinctive peaks of ZnO and hBN nanoparticles were identified, and as the hBN contribution increased, the peaks shifted and grew in size. As a result of FE-SEM analysis of ZnO nanoparticles, it was observed that the hBN nanorods grew significantly with the increase of hBN doping. It was also seen in EDX results that Zn, O, B and N contributions were successfully reached. As the amount of hBN reinforcement in the nanocomposites increased, a rise in dielectric constant was seen. This rise is assumed to be a result of nanocomposites' shifting load centers. The hBN addition to ZnO nanoparticles contributed to the improvement of the dielectric response. It was observed that the increase in hBN content led to a significant reduction in dielectric loss, and it provides a great potential for technological applications. Thus, the frequency stability of the dielectric properties improved after adding. For example, the variation of dielectric constant is 0.91 for pure hBN in the frequency range of 102 to 20 kHz, while it is only 0.39 for 10% ZnO doped composite. The electrical differences between ZnO-hBN nanoparticles lead to charge transport and accumulation at the interface. The resulting interfacial polarization leads to an increase in dielectric constant, dielectric loss and AC conductivity values. these composites can be one of the most fundamental materials with the potential applications in energy storage devices, solar cell production and photovoltaic devices.

Acknowledgements The authors thank the Firat University Research Fund (FUBAP-MF.21.74) for their financial contribution to this research and support. The produced nanoparticles in the study were applied to the Turkish Patent Institute with the title of “Hezagonal

Boron Nitride Reinforced Zinc Oxide Nanocomposite Materials and Preparation Method” with application number 2022/013404.

Author contributions T.G., C.K.M. and C.O. conceived the ideas. T.G., C.K.M. and C.O. produced samples and performed structural and morphological analyzes. F.B. and E.G. performed dielectric analysis procedures. T.G., C.K.M. and C.O. led the writing. T.G., C.K.M., C.O., F.B. and E.G. collected and analyzed the data. T.G., C.K.M., C.O., F.B., E.G. and S.B. designed the manuscript, worked with the graphic material, and edited and processed the manuscript. All authors have read and agreed to the published version of the manuscript.

Funding Open access funding provided by the Scientific and Technological Research Council of Türkiye (TÜBİTAK).

Data availability Not applicable.

Declarations

Conflict of interest The authors declare no conflict of interest.

Open Access This article is licensed under a Creative Commons Attribution 4.0 International License, which permits use, sharing, adaptation, distribution and reproduction in any medium or format, as long as you give appropriate credit to the original author(s) and the source, provide a link to the Creative Commons licence, and indicate if changes were made. The images or other third party material in this article are included in the article's Creative Commons licence, unless indicated otherwise in a credit line to the material. If material is not included in the article's Creative Commons licence and your intended use is not permitted by statutory regulation or exceeds the permitted use, you will need to obtain permission directly from the copyright holder. To view a copy of this licence, visit <http://creativecommons.org/licenses/by/4.0/>.

References

1. V. Mudavakkat, V. Atuchin, V. Kruchinin, A. Kayani, C. Ramana, *OptMa* **34**, 893 (2012)
2. C. Patel, B. Mandal, R.G. Jadhav et al., *ACS Appl. Nano Mater.* **5**, 2492 (2022)
3. M.O. Petrushkov, D.S. Abramkin, E.A. Emelyanov et al., *Nanomaterials* **12**, 4449 (2022)
4. T.S. Shamirzaev, V.V. Atuchin, *Nanomaterials* **13**, 2136 (2023)
5. T. Sahoo, M. Kim, J.H. Baek et al., *MaRBu* **46**, 525 (2011)
6. V. Garg, B.S. Sengar, G. Siddharth, S. Kumar, V.V. Atuchin, S. Mukherjee, *Surfaces Interfaces* **25**, 101146 (2021)
7. V. Mansurov, T. Malin, S. Teys, V. Atuchin, D. Milakhin, K. Zhuravlev, *Crystals* **12**, 1707 (2022)
8. C. Patel, R. Singh, M. Dubey et al., *ACS Appl. Nano Mater.* **5**, 9415 (2022)
9. D.S. Abramkin, M.O. Petrushkov, D.B. Bogomolov et al., *Nanomaterials* **13**, 910 (2023)
10. Z.L. Wang, *Mater. Today* **7**, 26 (2004)
11. M. Kahouli, A. Barhoumi, A. Bouzid, A. Al-Hajry, S. Guerrazi, *SuMi* **85**, 7 (2015)
12. V.K. Awasthi, S. Mukherjee, (2018)
13. H. Cheng, J. Cheng, Y. Zhang, Q.-M. Wang, *JCrGr* **299**, 34 (2007)
14. H. Serier, M. Gaudon, M. Menetrier, *Solid State Sci.* **11**, 1192 (2009)
15. A. Lotus, Y. Kang, J. Walker, R. Ramsier, G. Chase, *Mater. Sci. Eng. B* **166**, 61 (2010)

16. H. Cheng, X. Xu, H. Hng, J. Ma, *Ceram. Int.* **35**, 3067 (2009)
17. A. Verma, F. Khan, D. Kumar et al., *TSF* **518**, 2649 (2010)
18. R. Zamiri, A. Kaushal, A. Rebelo, J. Ferreira, *Ceram. Int.* **40**, 1635 (2014)
19. R. Zamiri, A. Lemos, A. Reblo, H.A. Ahangar, J. Ferreira, *Ceram. Int.* **40**, 523 (2014)
20. M. Dinesha, G. Prasanna, C. Naveen, H. Jayanna, *Indian J. Phys.* **87**, 147 (2013)
21. A.S. Adeleye, J.R. Conway, K. Garner, Y. Huang, Y. Su, A.A. Keller, *Chem. Eng. J.* **286**, 640 (2016)
22. W. Mai, Y. Zuo, X. Zhang et al., *ChCom* **55**, 10241 (2019)
23. J. Hassan, M. Ikram, A. Ul-Hamid, M. Imran, M. Aqeel, S. Ali, *Nanoscale Res. Lett.* **15**, 1 (2020)
24. Y.M. Lvov, P. Pattekari, X. Zhang, V. Torchilin, *Langmuir* **27**, 1212 (2011)
25. T. Saga, *NPG Asia Mater.* **2**, 96 (2010)
26. W. Lei, D. Liu, Y. Chen, *Adv. Mater. Interfaces* **2**, 1400529 (2015)
27. T. Han, F. Scarpa, N.L. Allan, *TSF* **632**, 35 (2017)
28. G.I. Giannopoulos, *SuMi* **115**, 1 (2018)
29. Y. Göncü, M. Geçgin, F. Bakan, N. Ay, *Mater. Sci. Eng. C* **79**, 343 (2017)
30. M.-H. Tsai, I.-H. Tseng, J.-C. Chiang, J.-J. Li, *ACS Appl. Mater. Interfaces* **6**, 8639 (2014)
31. N. Yang, C. Xu, J. Hou et al., *RSC Adv.* **6**, 18279 (2016)
32. C. Yuan, B. Duan, L. Li, B. Xie, M. Huang, X. Luo, *ACS Appl. Mater. Interfaces* **7**, 13000 (2015)
33. F. Rataboul, C. Nayral, M.-J. Casanove, A. Maisonnat, B. Chaudret, *J. Organomet. Chem.* **643**, 307 (2002)
34. E.A.S. Dimapilis, C.-S. Hsu, R.M.O. Mendoza, M.-C. Lu, *Sustain. Environ. Res.* **28**, 47 (2018)
35. T. Gurgenc, C.K. Macit, F. Biryani, E. Gurgenc, C. Ozel, S. Bellucci, *Appl. Phys. A* **129**, 649 (2023)
36. R. Raliya, J.C. Tarafdar, *Agric. Res.* **2**, 48 (2013)
37. S. Reda, *Mater. Sci. Semicond. Process.* **13**, 417 (2010)
38. C.S. Lim, A. Aleksandrovsky, M. Molokeev, A. Oreshonkov, V. Atuchin, *J. Solid State Chem.* **228**, 160 (2015)
39. C.S. Lim, A. Aleksandrovsky, M. Molokeev, A. Oreshonkov, V. Atuchin, *Crystals* **13**, 362 (2023)
40. K. Koran, F. Özen, F. Biryani, A.O. Görgülü, *JMoSt* **1105**, 135 (2016)
41. F. Bezgin, N. Ayaz, K. Demirelli, *J. Appl. Polym. Sci.* **132**, (2015)
42. L.-Z. Chen, D.-D. Huang, J.-Z. Ge, F.-M. Wang, *Inorg. Chim. Acta* **406**, 95 (2013)
43. C. Ramana, I. Troitskaia, S. Gromilov, V. Atuchin, *Ceram. Int.* **38**, 5251 (2012)
44. D. Vinnik, D. Klygach, V. Zhivulin et al., *JALIC* **755**, 177 (2018)
45. V. Grossman, V. Atuchin, B.G. Bazarov et al., *Molecules* **28**, 1629 (2023)
46. K. Koran, F. Özen, F. Biryani, K. Demirelli, A.O. Görgülü, *Inorg. Chim. Acta* **450**, 162 (2016)
47. S. Fratini, A. Morpurgo, S. Ciuchi, *JPCS* **69**, 2195 (2008)
48. A.-M. Haughey, B. Guilhabert, A.L. Kanibolotsky et al., *Sens. Actuators B: Chem.* **185**, 132 (2013)
49. Y. Tsai, F. Juang, T. Yang, M. Yokoyama, L. Ji, Y.-K. Su, *JPCS* **69**, 764 (2008)
50. R. Bokolia, O. Thakur, V.K. Rai, S. Sharma, K. Sreenivas, *Ceram. Int.* **41**, 6055 (2015)
51. C. Prajapati, P. Sahay, *Mater. Sci. Semicond. Process.* **16**, 200 (2013)
52. R. Zamiri, A. Zakaria, H.A. Ahangar, M. Darroudi, A.K. Zak, G.P. Drummen, *JALIC* **516**, 41 (2012)
53. X. Jia, M. Qin, W. Yang, *JMMM* **323**, 1423 (2011)
54. B. Santara, K. Imakita, M. Fujii, P. Giri, *JALIC* **661**, 331 (2016)
55. A. Shah, M.B. Ahamed, D. Neena, F. Mohmed, A. Iqbal, *JALIC* **606**, 164 (2014)
56. Y. Lin, C. Hsu, S.-K. Hung, C. Chang, D. Wen, *ApSS* **258**, 9891 (2012)
57. A.E. Kandjani, M.F. Tabriz, O.M. Moradi, H.R. Mehr, S.A. Kandjani, M. Vaezi, *JALIC* **509**, 7854 (2011)
58. S. Takahashi, Y. Imai, A. Kan, Y. Hotta, H. Ogawa, *JALIC* **615**, 141 (2014)
59. J. Gu, X. Meng, Y. Tang, Y. Li, Q. Zhuang, J. Kong, *Compos. A Appl. Sci. Manuf.* **92**, 27 (2017)
60. N. Ohba, K. Miwa, N. Nagasako, A. Fukumoto, *PhRvB* **63**, 115207 (2001)
61. R. Geick, C. Perry, G. Rupprecht, *PhRv* **146**, 543 (1966)
62. M.-H. Wang, Z.-Y. Zhao, T.-T. Liu, *JALIC* **621**, 220 (2015)
63. S.T. Gunday, E. Cevik, A. Yusuf, A. Bozkurt, *J. Energy Storage* **21**, 672 (2019)
64. W. Yang, J.J. Byun, J. Yang et al., *ACS Appl. Energy Mater.* **4**, 7959 (2021)
65. S. Madivalappa, V.M. Jali, A. Jain, *Macromolecular Symposia Wiley Online Library*, (2019)
66. L. Whittig, W. Allardice, *Methods Soil Anal. Part I Phys. Mineral. Methods* **5**, 331 (1986)
67. K. Mohanraj, D. Balasubramanian, J. Chandrasekaran, A.C. Bose, *Mater. Sci. Semicond. Process.* **79**, 74 (2018)
68. V. Mote, Y. Purushotham, B. Dole, *Mater. Des.* **96**, 99 (2016)
69. P. Singh, A. Kumar, A. Kaushal, D. Kaur, A. Pandey, R. Goyal, *Bull. Mater. Sci.* **31**, 573 (2008)
70. C. Zegadi, K. Abdelkebir, D. Chaumont, M. Adnane, S. Hamzaoui, *Adv. Mater. Phys. Chem.* **2014**, (2014)
71. N. Azizah, S. Muhammadiyah, M.A.K. Purbayanto et al., *Progress Nat. Sci. Mater. Int.* **30**, 28 (2020)
72. T. Gurgenc, *JMoSt* **1223**, 128990 (2021)
73. A. Sahai, N. Goswami, *Physica E* **58**, 130 (2014)
74. N. Goswami, D.K. Sharma, *Physica E* **42**, 1675 (2010)
75. Y. Ding, F. Torres-Davila, A. Khater, D. Nash, R. Blair, L. Tetard, *MRS Commun.* **8**, 1236 (2018)
76. M.C. Vu, T.S. Tran, Y.H. Bae et al., *Macromol. Res.* **26**, 521 (2018)
77. J. Li, X. Xiao, X. Xu et al., *Sci. Rep.* **3**, 3208 (2013)
78. B. Singh, G. Kaur, P. Singh et al., *Sci. Rep.* **6**, 1 (2016)
79. M.J. Akhtar, M. Ahamed, S. Kumar, M.M. Khan, J. Ahmad, S.A. Alrokayan, *Int. J. Nanomed.* **845**, (2012)
80. L.H. Li, Y. Chen, G. Behan, H. Zhang, M. Petravic, A.M. Glushenkov, *JMCh* **21**, 11862 (2011)
81. J. Hassan, M. Mahdi, S. Kasim, N.M. Ahmed, H. Abu Hassan, Z. Hassan, *ApPhL* **101**, (2012)
82. O. Hod, *J. Chem. Theory Comput.* **8**, 1360 (2012)
83. S. Senol, B. Yalcin, E. Ozugurlu, L. Arda, *Mater. Res. Express* **7**, 015079 (2020)
84. S. Roguai, A. Djelloul, *SSCom* **334**, 114362 (2021)
85. S. Roy, M.P. Ghosh, S. Mukherjee, *Appl. Phys. A* **127**, 451 (2021)
86. S. Saleem, M.H. Jameel, N. Akhtar et al., *Arab. J. Chem.* **15**, 103518 (2022)
87. M. Ahmad, E. Ahmed, W. Ahmed, A. Elhissi, Z. Hong, N. Khalid, *Ceram. Int.* **40**, 10085 (2014)
88. P. Labhane, L. Patle, G. Sonawane, S. Sonawane, *CPL* **710**, 70 (2018)
89. N. Kostoglou, K. Polychronopoulou, C. Rebholz (2015)
90. Q. Li, Z. Yang, Y. Miao et al., *RSC Adv.* **7**, 48994 (2017)
91. B. Niu, D. Cai, Z. Yang et al., *J. Eur. Ceram. Soc.* **39**, 539 (2019)
92. Z. Cui, Z. Cao, R. Ma, A.V. Dobrynin, D.H. Adamson, *ACS Appl. Mater. Interfaces* **7**, 16913 (2015)
93. K. Yang, X. Huang, L. Xie, C. Wu, P. Jiang, T. Tanaka, *Macromol. Rapid Commun.* **33**, 1921 (2012)

94. L. Xie, X. Huang, Y. Huang, K. Yang, P. Jiang, ACS Appl. Mater. Interfaces **5**, 1747 (2013)
95. Y. Yang, W. Guo, X. Wang, Z. Wang, J. Qi, Y. Zhang, Nano Lett. **12**, 1919 (2012)
96. M. Arshad, A.S. Ahmed, A. Azam, A. Naqvi, JALIC **577**, 469 (2013)
97. S.F. Junior, A. Souza, A. Peres et al., Appl. Phys. A **127**, 136 (2021)
98. S. Wang, D. Jia, Z. Yang, X. Duan, Z. Tian, Y. Zhou, Ceram. Int. **39**, 4231 (2013)
99. Y. Sun, Z. Yang, D. Cai et al., Ceram. Int. **43**, 8230 (2017)
100. A.S. Lanje, S.J. Sharma, R.S. Ningthoujam, J.-S. Ahn, R.B. Pode, Adv. Powder Technol. **24**, 331 (2013)
101. S.A. Mansour, R. Elsad, M. Izzularab, J. Polym. Res. **23**, 1 (2016)
102. M. El-Desoky, M. Ali, G. Afifi, H. Imam, M. Al-Assiri, SILICON **10**, 301 (2018)
103. T. Sharma, M. Garg, Eur. Phys. J. Plus **138**, 611 (2023)
104. Z. Tian, Y. Yang, Y. Wang, H. Wu, W. Liu, S. Wu, MatL **236**, 144 (2019)

Publisher's Note Springer Nature remains neutral with regard to jurisdictional claims in published maps and institutional affiliations.